THE SILICON LATTICE ACCELERATOR[*]

JAMES E. SPENCER[†]

Accelerator Research Department B, Stanford Linear Accelerator Center, 2575 Sand Hill Rd.
Menlo Park, California, 94025, USA

Previously, the generalized luminosity $\mathcal{L}$ was defined and calculated for all incident channels based on an NLC e^+e^- design. Alternatives were then considered to improve the differing beam-beam effects in the e^-e^-, $e\gamma$ and $\gamma\gamma$ channels. One example was tensor beams composed of bunchlets n_{ijk} implemented with a laser-driven, silicon accelerator based on micromachining techniques. Problems were considered and expressions given for radiative broadening due to bunchlet manipulation near the final focus to optimize luminosity via charge enhancement, neutralization or bunch shaping. Because the results were promising, we explore fully integrated structures that include sources, optics (for both light and particles) and acceleration in a common format - an accelerator-on-chip. Acceptable materials (and wavelengths) must allow velocity synchronism between many laser and electron pulses with optimal efficiency in high radiation environments. There are obvious control and cost advantages that accrue from using silicon structures if radiation effects can be made acceptable and the structures fabricated. Tests related to deep etching, fabrication and radiation effects on candidate amorphous and crystalline materials indicate Si($1.2 < \lambda_L < 10$ μm) and fused c-SiO$_2$($0.3 < \lambda_L < 4$ μm) to be ideal.

Keywords: lasers; damage; silicon; a,c-silica; luminosity; impedances; figures-of-merit; transmissive/reflective modes; parallel/serial structures; next generation lithography.

1. Introduction and Justification

Prediction is very difficult, especially about the future ... Niels Bohr

Like many systems today, accelerator energies have grown exponentially in time[1] and, in most cases, the growth has come at the cost of complexity. However, in most of these, cost and reliability have improved due to reduced size as well as increased production and integration. In contrast, next-generation, high-energy machines will be very complex and expensive with a poor risk-reward outlook because of their one-of-a-kind nature. In the early-eighties, with the advent of the linear collider, it became apparent that a better predictive measure than the Livingston plot was needed to forecast the future and thereby motivate new developments. One attempt[2] compared the growth in complexity of single chip microprocessors and electron storage rings where it was argued that there was a correlation between these curves in that such micros or their equivalents were necessary for the rings to operate. The SLC was not shown but was thought to have a higher complexity.

[†]Email Address: jus@slac.stanford.edu

The slopes of these curves are remarkably similar and close to Livingston's analysis[1] of a 10-fold increase in energy every six years up to 1960. They were based on the first commercial availability of the chips and the first published physics. Later, single-chip, dynamic random access memory and proton storage rings were added[3] showing DRAM to have a much faster growth rate and the proton rings a much slower one than Tigner's in terms of constituent energy. Adding the proposed LHC and SSC rings indicated a date of 2008 for the SSC in 1990. Extrapolations for the Intel micros have been consistent with Moore's rule since that time.

In the last decade, there were two important technologies that drove these and other comparable advances. Semiconductor fabrication techniques and related laser developments were also applied in telecommunications and many other areas and they can be expected to be more closely integrated into more compact and novel devices during this decade. Of special interest is the micromachining of Si using conventional semiconductor foundry techniques because of its potential use for MEMS. New laser systems and their uses are growing even faster. In materials processing they are now used to drill, perforate, weld, anneal, clean and polish. Combining these two with their economies-of-scale provides a powerful incentive to use them in the next generation machine for high energy physics.

If this story is to have a good outcome, the initial conditions are important. Here, the source embodies all the technology and sets the limits on the outcome. In many respects, it is the hardest part of the problem but has the most important technological payoffs so it will be the main focus after reviewing prior results and a few important fundamentals related to the acceleration process.

2. Basic Concepts, Characteristics and Parameters

One can understand the laser acceleration problem in a consistent way for both particles and fields as well as conventional RF accelerators where the waveguides are conducting with much higher complex permittivities at RF. The limiting factor on the acceleration gradient is the electric field damage threshold of a material. Structures made from dielectric materials are typically expected to provide an order of magnitude improvement over what has been achieved with conventional RF. Phase space volumes, phase and group velocities, emittance as well as electrical and optical impedances are common characteristics as are their scaling and combinatorics. We will use 'bunchlet' for electron pulses, 'wavelet' for laser pulses or 'packet' when there is no distinction.

2.1. *Figures-of-Merit*

2.1.1. *Luminosity*

The most important figure-of-merit for colliders is the total, integrated, usable luminosity. The generalized luminosity[4,5] was based on the observation that **all** colliding beam machines as well as **all** incident channels in any particular GLC

can be expected to have a luminosity proportional to the square of the *primary*, incident bunch 'charge' (N_B^2 or $n_B N_B^2$ or $n_x n_y n_z N_B^2$ or $n_z(n_x n_y N_B)^2$) that can be brought into collision per unit time within an effective area that contains the *effective* number $\widehat{N}_B$ based on conversion efficiencies and detector constraints[4,5,6]. For a laser driven accelerator, where the laser and electron normalized emittances are matched, one can write, in terms of the standard NLC expression

$$\mathcal{L} \; = \; \frac{f_r n_B N_B^2 H_D}{4\pi\sigma_x^*\sigma_y^*}\zeta \equiv \mathcal{L}_G H_D \zeta \; \rightarrow \; \frac{f_r n_B N_B^2 \gamma H_D}{4\pi\epsilon_n\beta^*} \; \zeta \; \propto \; \frac{P_b}{\lambda Z_R}N_B H_D \zeta \qquad (1)$$

where the various parameters are the usual ones[4,5,6] e.g. $\sigma_{x,y}^*$ is the undisrupted, rms spot size at the interaction point and β^* is the magneto-optical 'depth-of-field' at the IP. The arrow simplifies to round beams and $P_b \propto fnNE_b$ is the incident, primary electron beam power. β^* is equivalent to the Rayleigh range $Z_R > \lambda$, the laser wavelength. In this scenario, luminosity increases with decreasing λ^2.

2.1.2. *Impedances*

We also know that $\mathcal{L}$ is directly proportional to the available power to accelerate the primary beams. The on-axis, unloaded gradient of an accelerator cell can be defined as

$$G_U \; = \; \frac{\sqrt{PZ_c}}{\lambda} \; \overset{1.5\mu m}{\longrightarrow} \; G_U[MeV/m] = \sqrt{P[W]} \; \text{ for } Z_c = 2.25\Omega \qquad (2)$$

which defines the characteristic impedance Z_c of the structure's accelerating mode. Z_c can vary greatly but gives a reasonable benchmark. The peak power is determined by the structure's damage threshold but commercial sources[7] are available that can provide 50 MHz rep rates. This expression implies that a shorter wavelength is preferred over power or impedance but if power or efficiency was not a problem we could get any $\mathcal{L}$ we could use. Any choice of λ assumes that one has the power source and the means to fabricate structures to the required tolerances that can withstand the power. With the rapid development of high power lasers and micromachining techniques we have a good justification for the LEAP project[8] if we do the materials science properly.

If we assume that a fixed power is available to us in some form[a] we can enhance Z_c by series addition of cells to improve energy gain per unit power by $\sqrt{n_c}$

$$E_b \; = \; \sum_{n_c} \frac{l_c}{\lambda}\sqrt{\frac{P}{n_c}Z_c} \; = \; l_c\sqrt{n_c}G_U \; . \qquad (3)$$

l_c is the acceptable slippage distance between bunchlet and wavelet $\leq \lambda/2(1-\beta)$. This increases accelerator length and it will become clear that adding cells in parallel

---

[a]A logical solution that might justify a US site for the NLC would be to build it near the Yucca Mountain waste site. At the same time, build a nuclear power complex nearby that is also convenient to the national power grid. The NLC exhaust beam could be used for waste transmutation.

improves efficiency. The impedance of this parallel pathway Z_T for any wavelet effectively determines the so-called shunt impedance as well as the allowable number of parallel bunchlets. It is determined by Z_c and the transmittance $T(\lambda)$ of the structure between cells. As will be shown, T can be large for silicon (or silica) for laser wavelengths $\lambda > 1.2\mu$ when we couple the beam into these materials properly.

From reciprocity, every force implies some damping e.g. one cannot accelerate without radiation or retardation effects. The beam excites higher modes that dissipate beam energy and this provides another impedance Z_h that leads to a loaded gradient G_L that is not less than half G_U but depends on the charge per bunch desired. This is another justification for tensor beams that can reduce the charge per bunchlet. Clearly, we want to increase Z_c, reduce Z_h and maximize T.

2.1.3. *Brightness and other measures and constraints*

While $\mathcal{L}$ and the impedances associated with the accelerator are important, we know that there are many subsystems with their own FoMs and one of the most important concepts where misunderstanding occurs relates directly to the beam itself. Liouville's theorem and the Vlasov equation, in varying approximations, place good lower bounds on what is ultimately achievable and is why we have emphasized the importance of the source. However, it is also relevant to the bunchlets we want to propagate, combine and/or neutralize.

While there are far more questions than we can answer here, it is important to note that the only meaningful statement for the distribution function in terms of the canonical variables in six dimensional phase space is that the *local* density is an invariant. This assumes noninteracting particles even though they collide and interact through collective space charge and self magnetic fields whose influence varies with energy. However, the former are negligible compared with the smoothed fields of the latter when the Debye length is 'large' i.e. $n\lambda_D^3 \gg 1$ or the number of particles in a Debye sphere is large. This is often the case and will be assumed.

Thus, control of the 6 dimensional phase space of the particle beams required for high energy colliders must begin with production and proceed through every subsequent step from bunching, compression, acceleration, application and disposal. During each of these steps, different mechanisms act to increase the phase space in irreversable ways. During production, preacceleration and matching into the main accelerator, space charge effects become increasingly important with frequency. This is especially true for the frequencies implied for laser driven accelerators where both the microbunch lengths and transverse emittances should all be a fraction ($\approx \frac{\lambda}{4\pi}$) of the optical wavelength. While this apparently argues in favor of longer wavelength lasers, the problem is significant for any laser wavelength and therefore implies that new techniques are needed before any of the new high-gradient, high-frequency acceleration schemes that are currently under consideration become feasible.

We discuss this in a later section, where various projections are calculated for the lattice accelerator and compared to a collider configuration. The quantity that best

represents the fully invariant 6D phase space for linear, time independent systems is the normalized brightness:

$$B_n^6 \; = \; \frac{N_B}{\epsilon_{nx}\epsilon_{ny}\sigma_z\sigma_\gamma}$$
(4)

where σ_z and σ_γ are the bunchlet's rms length and energy spread.

2.2. *Dielectric loaded waveguide/accelerator*

Whether one has a disc or dielectric loaded waveguide structure, the modes can be classified as transverse magnetic TM_{jlm} with $E_z \neq 0$ and $B_z \equiv 0$. For cylindrical symmetry, this implies p polarized wavelets. For waves of finite extent, the group velocity in any direction is $v_g < c$ - superluminal, technical anomalies aside. From the waveguide mode dispersion equation or simple geometric arguments one has, above cutoff,

$$\beta_g = \frac{v_g}{c} = \sqrt{1 - (\frac{\nu_c}{\nu})^2} \; = \frac{c}{v_p} \quad \ni \quad v_g v_p = \frac{c^2}{n^2} = \frac{1}{\epsilon\mu} \; .$$
(5)

where the cutoff frequency, ν_c is, quite generally, given by the guide's cross section:

$$\nu_c = \frac{c}{n}\sqrt{\left(\frac{j}{2a}\right)^2 + \left(\frac{l}{2b}\right)^2}$$
(6)

for a rectangular guide, pseudo-planar circuit etc. with n an effective value defined by the mode and circuit characteristics. Note that a mode's unloaded, lossless wave impedance in vacuum is $Z_{TM} = (E/H)_{xy} = \beta_g Z_0$. We want v_p close to c i.e. $\nu \gg \nu_c$ because this increases the slippage distance or guide length. For sufficiently high energies:

$$v_p/c = \lambda_{wg}/\lambda = \sqrt{\frac{1}{1 - (\lambda/\lambda_c)^2}} \; \leq \gamma^2 \; .$$
(7)

This ratio is determined by varying the cell length for a given laser λ, aperture and crossing angle to optimize energy gain. One concludes that we must either increase λ_c i.e. the guide size or decrease λ - neither of which is very agreeable except for the very large changes achievable with lasers. This is what LEAP[8] is exploring.

An old idea is to load the waveguide with dielectric[9]. For small apertures:

$$v_p/c = \lambda_{wg}/\lambda = \sqrt{\frac{1}{\epsilon_r\mu_r - (\lambda/\lambda_c)^2}} \; \leq \gamma^2 \; .$$
(8)

This suggests a graded index. Increasing either ϵ_r or μ_r from their vacuum values provides useful knobs allowing a smaller waveguide and higher accelerating fields. Problems include variable capacitance through charge buildup from lost electrons, dielectric breakdown and aging from poor heat dissipation or radiation damage.

2.3. *The Importance of Reflectance*

In contrast to RF approaches, the reflectance, transmittance and absorptance, with $R + T + A = 1$, are important to every part of our problem. Thus, the expressions above are generally valid and, in a geometric picture, they can be thought of as defining the mean angle of propagation of the fundamental mode down the guide i.e. $\beta_g \equiv cos\theta_c$. For conventional metallic guides, the characteristic angle $\theta_c = 90°$ defines the cutoff frequency where there is no propagation down the guide. For consistency with optical conventions, we will rotate our angle reference by $90°$ because the guide surface is more relevant than its axis. Thus, normal incidence, defining $k_\perp \equiv k$, now occurs at $0°$.

Brewster's angle $\theta_B > 52°$ for the wavelengths and dielectrics or semiconductors of interest here so this angle defines the onset of the parallel, transmission mode while R and the number of reflections per unit length determines the extinction rate of the serial, reflective mode for smaller angles and thereby the serial shunt impedance Z_R as opposed to Z_T mentioned earlier.

Dielectrics have nearly zero absorptance while metals always have greater than zero. Polished metals thicker than ≈ 50 nm can have high reflectances up to 98% at normal incidence while uncoated dielectrics such as glass typically have 4-8% but the addition of a single, quarter-wave layer of intermediate index material can reduce this to <1%. This is an example of impedance matching where R can be thought of as resulting from some mismatch. It depends on the materials, their thickness l, the angle of incidence, wavelet polarization, surface structure and incident intensity.

2.4. *Damage mechanisms*

In our materials damage studies, we scan a light beam of variable frequency ω at normal incidence on flat polished surfaces and measure $R(\omega)$ and $T(\omega)$ as functions of differing thicknesses d, intensities I_k and doses D_l of γs and/or neutrons. For single reflections i.e. first order or reflections from an infinite half-plane, one has, in direct analogy to a terminated impedance

$$R(\omega, \theta, P, \epsilon_j, \mu_j, I_k, E_{BG}, D_l, t) = \frac{(Z_2 - Z_1)(Z_2 - Z_1)^*}{(Z_2 + Z_1)(Z_2 + Z_1)^*} \xrightarrow{0°} \frac{|(n_2 - n_1)|^2}{|(n_2 + n_1)|^2} \quad (9)$$

with P the wavelet polarization, E_{BG} the bandgap energy, $Z_j(\omega) \equiv (\mu_j/\epsilon_j)^{1/2}$ the complex wave impedance. If n_{0j} is the index of refraction, the complex index n_j is

$$n_j(\omega) \equiv (\mu_{rj}\epsilon_{rj})^{1/2} = n_{0j}(\omega) + ik_{0j}(\omega) + n_{2j}(\omega)I(\omega) + \cdots \quad (10)$$

where k_{0j} is the index of extinction and the sign and magnitude of the nonlinear term n_{2j} can provide a variable lensing action. This term is responsible for laser damage effects through multiphoton ionization processes e.g. $m\hbar\omega \geq E_{BG}$ or through self focussing effects[10] that increase the effective intensity I.

Radiation damage is often specific to the type of radiation as well as integrated dose. Materials age, damage, anneal, relax, absorb or adsorb other materials in

ways that can seriously change their properties in time dependent ways. Usually, such changes show a strong frequency dependence as with the diffusion of hydrogen into or out of silica or the growth of color centers from crystal dislocations.

2.5. *The Generalized Luminosity $\mathcal{L}$*

For a 'tensor' accelerator, we add two transverse variables (n_x, n_y) to the basic luminosity expression Eq. 1. These count the number of 'accelerators' or beams in the transverse plane. $n_q(=1$ or $2)$ gives the number of charge species in a bunchlet N_B and the number of bunchlets in any one train becomes $n_z=n_B$. The generalized luminosity is then:

$$\mathcal{L} \;=\; \frac{n_x n_y n_z}{n_q} \frac{f_T (N_B n_q)^2 H_D}{4\pi \sigma_x^* \sigma_y^*} \zeta \;=\; n_x n_y n_z n_q \frac{f_T \widehat{N}_B^2}{4\pi \widehat{\sigma}_x \widehat{\sigma}_y} \zeta' \;. \tag{11}$$

This is a good example of why we specifically avoided labels on the luminosity or the number of electrons in a bunch N_B. An example was illustrated in Ref. 5 that took advantage of silicon, integrated circuit technology to achieve charge compensation that could curtail beamsstrahlung. There we took $n_x= 2n_y=2$ and accelerated equal bunches of e^+ and e^-, to give

$$\mathcal{L}(n_x{=}2, n_y{=}1, n_z{=}1, \ n_q{=}2) = 4\mathcal{L}(n_x{=}n_y{=}n_z{=}n_q{=}1) = \mathcal{L}(e^-e^-) + 2\mathcal{L}(e^+e^-) + \mathcal{L}(e^+e^+)$$

assuming perfect alignment and charge compensation but no enhancement. Clearly, higher luminosities are possible in any number of conceivable configurations. With less than one event per crossing and good charge discrimination, this should be a viable operating configuration capable of new physics.

3. A Schematic Cell Example

Figure 1 shows a possible cell for a parallel, transmissive structure. In this planar view, linearly-polarized laser beams are crossed in the cell to provide a longitudinal accelerating field. The light enters on the top and exits at the bottom at the Brewster angle θ_B in such a way that it can then be reused to improve efficiency.

Using integrated circuit techniques, one can as easily fabricate these structures into an array or matrix over a single wafer. Light from high-power, diode-pumped lasers can be split into several parts (e.g. n_z) for multicell, tensor acceleration as shown in Fig. 5 of Ref. 5. In that example, we illustrated charge compensation with $n_x=2$, $n_y=1$ and $n_q=2$ using equal bunches of e^+ and e^- to give $\mathcal{L} \approx 4\mathcal{L}(e^+e^-)$ as discussed in Sect. 2.5.

Unfortunately, for fabrication in Si, this cell has certain shortcomings. First, it is clear from Sect. 2.3 that there are three times more reflections per bunchlet crossing than necessary. This introduces the so-called critical angle θ_{cr} for internal reflection as a constraint where the reflectance $R{\to}1$ independent of wavelet polarization when the transmitted angle $\theta_t{\to}90°$. For our glass example, with n=1.5, this angle is $\theta_{cr}{\approx}42°$. Similarly, for conventional foundry fabrication in Si when we want $n_y> 1$ we need to use (110)-wafers for anisotropic etching. In this case it is necessary to orient the entrance and exit Brewster faces parallel to the large vertical faces, where

the bunchlets cross at the perpendicular, so that all of these can be oriented parallel to the [111] line in the wafer as shown next.
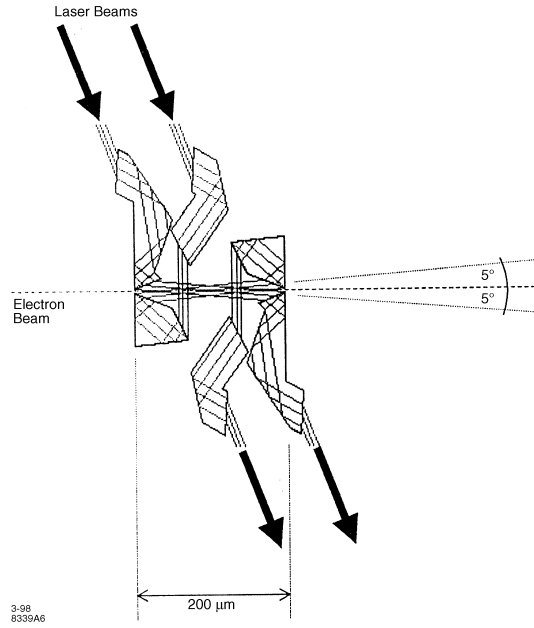

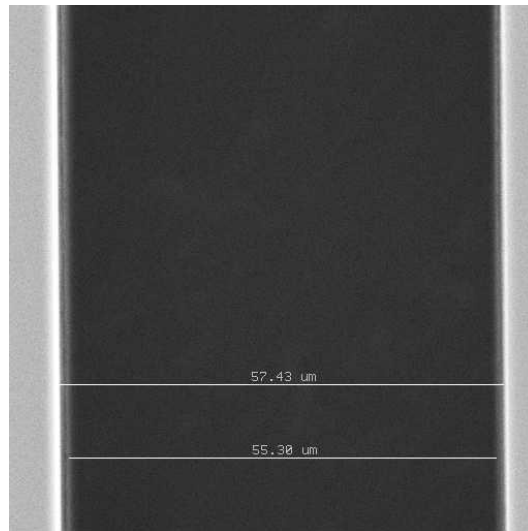Fig. 1.   Schematic, planar view of a possible single, side-coupled laser accelerator cell.

Fig. 2.   View of a 50 μm slit etched along the [111] line in a 500 μm thick, (110) Si wafer. This demonstrates a wall height-to-thickness ratio of 500:1. Thinner line widths are harder to view and thicker ones have worse resolution.

4. Results of Deep Etching Studies

Because these structures are to be fabricated in Si, there is an important question of whether they can be made deep enough to accommodate a true tensor structure with $n_y > 1$. In Fig. 2 we demonstrate that it is possible to etch a single, thick wafer **or** a stack of such wafers using the same technology to provide accurate registration between wafers. Although one can use IR light through surface features for relative alignment purposes, this does not provide sufficient resolution. This will become evident later.

In this and similar SEM pictures, we demonstrated that it is possible to go from an unknown [111] orientation on a (110) wafer to make small accurate slits with length-to-width ratios of 250:1 and wall height-to-width ratios of 500:1. We also demonstrated that the surface of the walls were flat, parallel and smooth to better than $\approx$10 nm by finding and focusing on particles < 100 nm in size that were left on the surface of the walls.

Previously, we showed[5] that one can combine a vertical stack of bunchlets into a single, flat bunch with charge $n_y N_B$ with minimal radiative effects. Alternatively, we could simply accelerate flat beams using cylindrical lenses. This is clearly the simpler option to fabricate and provide beams for. Under the same assumptions as used above, one expects a luminosity $\mathcal{L} \approx 4n_y^2 \mathcal{L}(e^+e^-)$. However, if we decrease N_B, we must then increase n_y to maintain the same total luminosity $\mathcal{L}$.

Fig. 3.   Transmission spectra through a 6.35 mm thick, polished, silica cell as a function of dose.

5. Representative Damage Examples and Results

Amorphous, fused silica (a-SiO$_2$) is an ideal but complex example that finds many applications. It was used for our first accelerator cells[8,11] due to its ease of use and good thermal stability that provides the potential for stable, high-reflector coatings under high power beams. Because it has a high bandpass over our full wavelength range, it has many uses that make its transmission characteristics and their stability important. Figure 3 shows the measured transmission spectra for an uncoated, machined and polished accelerator cell from CVI Laser[12] as a function of total Co^{60} γ-dose in Si equivalents.

The maximum transmission here is T>94 % at 1600 nm with four prominent absorption regions near 210, 1385, 2210 and 2760 nm or in frequency: 47,620, 7,220, 4,524 and 3,622 cm^{-1}. The most interesting of these is the activation dip at 212 nm (5.84 eV). The observed damage is roughly linear at

$$T(212 \text{ nm}) = 0.823 - 1.36 \cdot \text{Dose(MGy)} \tag{12}$$

An example of crystalline data is shown in Fig. 4 for comparable thickness wafers of quartz (c-SiO$_2$) and silicon. There is no evidence for damage in any Si sample up to 9 mm thickness for γ-doses up to 325 kGy. Similarly, there is virtually no damage to the quartz except in the near-UV below 300 nm where the damage goes as $T(212)$=0.908-0.539·Dose(MGy) - much better than for the amorphous silica (a-SiO$_2$) shown in Fig 3. Si samples with t=0.5, 3 and 9 mm gave identical results.

Fig. 4.   Transmission spectra through Silicon and Quartz wafers as a function of integrated dose.

Because glass shows serious damage under low proton[13] as well as γ-doses, we

must eliminate it for many uses. Fortunately, the quartz and silicon are quite acceptable at current levels. Clearly, neutron displacement studies are now of interest. We conclude that pure amorphous materials are preferred over typical glasses and pure crystalline materials are preferred over the pure amorphous because of the latter's greater number of states and structural characteristics such as greater susceptibility to permeation. It will be interesting to see whether these conclusions remain after neutron displacement studies. These are being pursued together with a broad array of fiber optic, laser, optical coating and other materials.

6. Tensor Source and Laser Driver

For conventional radio frequency accelerators, the rf gun was a major improvement that was well matched to the rf accelerator. Increasing rf frequency improves the situation because it allows higher gradients that increase the inertial resistance to space charge blowup out of the cathode as well as helps to avoid bunching systems. However, if a buncher is required, as for laser based acceleration frequencies employing conventional rf guns, then space charge debunching and transverse blowup appears difficult to avoid. This remains true even when the microbunch charge is considerably reduced. Thus, laser acceleration schemes require new source techniques compatible with the new wavelength regime.

A generic drive laser system such as required is suggested in Fig. 5 where the laser depends on the system to be driven. It could be used, in various forms, to drive a pin-cushion cathode to produce tensor beams or as a power source for the accelerator where Ti:Sa, Er:YAG and Cr:ZnSe are possible candidates.
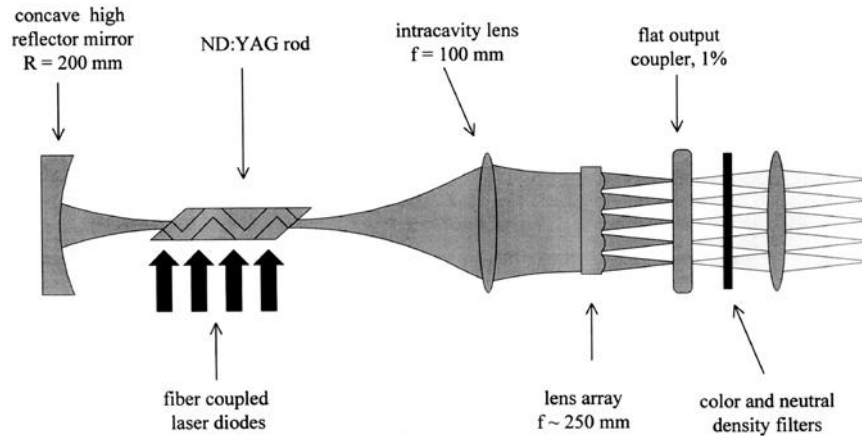

Fig. 5.   Schematic of a multibunch laser driver for both source and accelerator.

Figure 6 shows a cross-sectional view of a possible implementation of a tensor cathode. A matrix of sharp-tip cathodes are biased relative to a gated, anode grid

and illuminated on the back by a laser to provide sufficient energy to generate cold, field-emitted electron bunches.

This generic structure is comprised of a grid of anode holes and a separate grid of cathode tips bonded together with indium. An array of tiny holes in a membrane of silicon nitride coated with a thin layer of gold is used as an anode. The cathode may be a micro-machined array of tips that can be coated with any material to improve emissivity and durability. An array of lenses is micro-machined under each cathode tip and focuses incident radiation onto the tips. The lens array is not strictly focusing since the tips can be used as non-imaging collectors or refractive concentrators, but lenses can improve the efficiency of light collection at the tips. There are several ways of aligning the two pieces before bonding them together. In the implementation shown in Fig. 6, a fiber is placed in a v-groove on the cathode array and it locks into a corresponding v-groove on the anode piece. Heating the combined pieces to 170° C melts the indium and bonds the two pieces together. Applying a bias between the tips and the anode grid and illuminating the tips with laser radiation will then induce a flow of electrons from each tip.

A broad range of materials can be studied together with their distributions of emitted electrons that are generated based on differing structures and excitations. Note that tips may not be necessary for some materials such as GaAs and that this may well be advisable from the standpoint of stability and lifetime but these characteristics will depend on the applied voltages, wavelengths and intensities. Polarized beams can also be generated using circularly polarized light. STM probes produce about 4 pA/V of ballistic electrons from GaAs with no laser light whatsoever in a technique called ballistic electron emission microscopy.
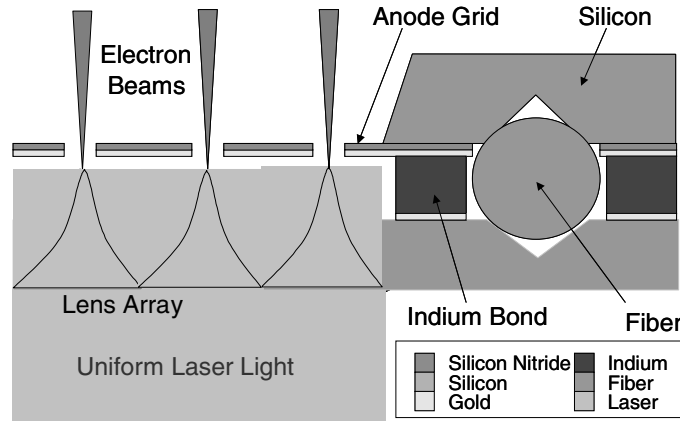

Fig. 6.   A highly schematic layout for a backlit, gated photocathode.

There are many different potential implementations of the matrix cathode. We have considered three architectures that might be promising. One involves using

near-infrared (NIR) radiation and silicon as a transparent material. The other silicon-based structure hollows out the tips so that any wavelength can be used. The final structure uses a wafer of fused silica that allows for any practical energy. We will discuss only the latter two and one important practical application.

7. Hollow Silicon Structure

Figure 7 shows the fabrication procedure for the hollow matrix cathode. As with the transparent structure, we begin by patterning a 500 nm thick layer of silicon nitride on both sides of a double-side polished silicon wafer. We pattern the top surface with photolithography and a CF_4/O_2 plasma in Step 1. The wafer is then placed in KOH to form an array of sharp tips. We then coat the tips and the silicon nitride at the side with a layer of gold. To complete Step 2, we coat the gold with a thin layer of molybdenum e.g. in a high vacuum sputter source. In Step 3, we pattern the silicon nitride on the back surface and place it in potassium hydroxide to etch holes in the silicon in Step 4. In Step 5 we protect the gold on the front with photoresist and then etch the gold from the underside of the molybdenum tips. Finally, we remove the photoresist and plate indium for bonding in Step 6. The tips can be fabricated with four sides having 45° sidewalls or with eight sides having 76° walls.

Fig. 7.   Fabrication procedure for a hollow, silicon matrix photocathode.

8. Fused Silica (c-SiO$_2$) Structure

Figure 8 shows the fabrication procedure for the silica matrix cathode. As before, we coat both sides with 500nm of silicon nitride and pattern pillars of photoresist on the wafer. We then thermally reflow the photoresist in Step 2 to form spherical lenses of photoresist. In Step 3, we transfer the photoresist lenses into the silica with a CF_4/O_2 plasma etch. We then pattern the silicon nitride on the front surface using

photoresist and a CF_4/O_2 plasma. Using a hydrofluoric acid etch, we form the tips shown in Step 5. As with the silicon structure, the silicon nitride will float away when the etchant terminates. In Step 6, we pattern gold on the edge and plate it with silicon nitride.

Fig. 8.   Fabrication procedure for a fused silica, quartz matrix photocathode.

9. Comparison to NLC

In Sect. 2.1.3 we defined the normalized brightness, which is difficult to measure, and is usually integrated over one or more dimensions to provide (Poincare Invariants) something that is more easily measured or of more direct interest such as the transverse or longitudinal equivalents:

$$B_{nt}^{(5)} \;=\; \frac{I_B}{\epsilon_{nx}\epsilon_{ny}} \quad \text{and} \quad B_{nl}^{(2)} \;=\; \frac{I_B}{\sigma_\gamma} \;. \tag{13}$$

Nevertheless, while these invariant projections are more common, $B_n^{(6)}$ is the best general measure of beam or bunchlet quality that one would like to conserve. We can "coalesce" bunches in any way we want as long as we don't violate Hamilton's or Maxwell's equations for the assumed external fields.

It is interesting to compare a nominal Si lattice and an NLC design to check its relevance for this or other applications at much lower energies. We have indicated its relevance for polarized beams and that it does not require damping rings as needed for rf guns. Further, we will not take advantage of the fact that crossing angles are not required nor any of the luminosity enhancements that implies[4,5,6].

Table 1 shows results for a lattice that is arbitrarily scaled to NLC to show that parameters such as $\mathcal{L}$, $D_{x,y}$ or Υ remain reasonable. It is also interesting for low energy applications. The results become more interesting when one realizes that the NLC is supposed to operate at $n_B f_{\text{rep}}$=16 kHz[14,4,5] while the Si laser lattice has the potential[7] of 50·n_x MHz.

Table 1: Comparison of NLC500A[14,4,5] and Silicon Lattice at E_{cm}=500 GeV.

Parameters	500A	Si Lattice	Comments
N_B [10^9]	6.5	0.065	nominal 1 nC for NLC
$\epsilon_{nx}/\epsilon_{ny}$ [μm]	5/0.08	0.01/0.01	normalized emittances
β_x^*/β_y^* [mm]	8/0.125	0.5/0.5	beta function at IP
σ_x^*/σ_y^* [nm]	286/4.5	3.2/3.2	rms bunch sizes at the IP
σ_z [μm]	100	3	rms bunch length
σ_γ/γ [%]	0.1	0.5	relative rms energy spread
$(|D_x|/|D_y|)$	0.090/5.70	0.22/0.22	disruptions
$\mathcal{L}_G$[10^{33}m^{-2}sec^{-1}]	2.6	0.033	geometric $\mathcal{L}_G$/bunchlet
$\mathcal{L}_G^r$[10^{33}m^{-2}sec^{-1}]	2.6	0.13	flat beam $\mathcal{L}_G$/bunchlet
Υ	(0.10)	(2.5)	strong field parameter
H$_D{\equiv}\mathcal{L}_{e\pm}/\mathcal{L}_G$	1.42	1.0	$\mathcal{L}(e^+e^-)$ enhancement
$\mathcal{L}_{e\pm}$[10^{33}m^{-2}sec^{-1}]	3.7	0.13	$\mathcal{L}(e^+e^-)$/bunchlet
H$_D{\equiv}\mathcal{L}/\mathcal{L}_G$	0.55	1.0	$\mathcal{L}(e^-e^-)$ enhancement
$\mathcal{L}_{e^-e^-}$[10^{33}m^{-2}sec^{-1}]	1.43	0.13	$\mathcal{L}(e^-e^-)$/bunchlet
$\delta z/\delta z_{in}$	10^{14}	240-1 MeV	ballistic bunching distance
B_n^6 [m^{-3}]	3·10^{23}	2·10^{31}	normalized 6D brightness
B_{nt}^5 [A/m^2]	3·10^{15}	4·10^{18}	normalized 5D transverse
B_{nl}^2 [A]	3	45257	normalized 2D longitudinal

In the Table, the scaling to flat beams is based on taking the ratio r=$\epsilon_y/(\epsilon_x + \epsilon_y)$ while holding $(\epsilon_x + \epsilon_y)$ constant. Scaling the luminosity by $1/\sqrt{r(1-r)}$ then gives a fourfold gain compared to round beams using the same r as for NLC.

The ballistic bunching ratio of 240 at 1 MeV was determined by assuming that one can impose a longitudinal position-energy correlation and then simply calculating the ratio $\beta_h/(\beta_t\text{-}\beta_h)$ where β_h is the relative velocity at the head. For the bunch length to approach zero, in the absence of space charge, it requires a drift length of 240 times the bunch length.

10. Practical Applications

Some important possibilities include Optical-Electrical-Optical (OEO) 'switches', magnetic recording and e-beam lithography. Because the first two are heavily materials specific, only the latter will be discussed here. This is especially appropriate if, as claimed, increasing collider energies rely in some essential way on Moore's law. Further, space charge and higher order aberrations are an overriding concern here although simpler to implement because one can have a matrix cross section whose size is that of the wafer ($\leq$ 30 cm). Currently, there are at least three possibilities for next generation lithography (NGL):

- Deep Ultraviolet (DUV),
- Extreme Ultraviolet (EUV)[15],
- Projection e-beam[16], and

• Direct write e-beam[17].

Feature sizes as low as 0.13 μm for gate lengths in microprocessors are the current standard based on 193 nm lasers. If current goals and history persist, one expects the minimum feature size to halve every six years or 65 nm by 2007 and 32 by 2013. Traditional optical sources achieve feature resolution at the expense of the depth-of-field since from the Rayleigh equations $R\propto\lambda$/NA whereas $DoF=R$/NA. DUV allows some alternative optics options e.g. transmissive at 157 nm but EUV does not. Thus, just as for the reflective or serial accelerator cell, high reflector coatings are necessary but presumably much easier to implement for EUV lithography.

The E-beam option would seem to be the ideal NGL choice because 10-100 KeV beams are readily available that are not diffraction limited with wavelength e.g. λ_e(10 keV)=0.24 Angstroms whereas a 50 keV photon would be required. It is not unreasonable to assume that the former is more easily attainable. Projective e-beam uses conventional electron optics to produce 250 μm square beams on a thin Si mask. Interestingly, all of the "Big-Three" use masks fabricated by direct write e-beams on the same materials of interest to us here - Si and fused c-SiO$_2$ with beams in the range of 5-100 nm diameters.

The problem, of course, is throughput for semiconductor manufacturing where the gates and contacts cover 50 % of the wafer. While there are many strategies on how to use the e-beam such as raster or vector scanning over a stage that may be stationary or moving, there has been no proposal to use tensor beams. Instead, the discussion typically involves improving e-beam currents or polymer sensitivity to achieve optimum doses[18] of 5-10 μC/cm^2 per step. In Table 1, we assumed 10 pC/pulse. For 100 keV electrons, this implies 250 μC/cm^2/pulse at a rate of up to 50 MHz. This gives sufficient time to vary the optics between steps over a square matrix $n_x \cdot n_y$ which determines the throughput because we have made and tested Si based electron optics at the 10 μm scale capable of carrying 1 A, 50 ns pulses. A pulse length and beta function of 1.2 μm gives a spot $\sigma_{x,y}$=100 nm and this can be reduced dramatically. Clearly, the wafer layout and stepping strategy is critical.

11. Conclusions

Because one doesn't know what the ultimate wavelength or pitch can be, a somewhat arbitrary Si configuration was assumed in Table 1 for easy scaling with NLC. Even though the bunchlet current was less than a third of the NLC value, all of the brightness measures heavily favored the Si lattice. Further, we can easily reduce both the bunchlet charge and length by 10 or more without much harm to the conclusions. These are that Si, in various forms, is a remarkably good material for such applications in every way that has been checked. It also follows that mask costs could be reduced dramatically quite apart from any lithographic applications.

Nevertheless, charge compensation schemes and bunch shaping that have been discussed previously are especially important to improve $\mathcal{L}$ in the different channels[5,6] but also to cancel transverse, space charge effects between bunchlets during acceler-

ation. Typically, even the central bunchlet in an array is not fully immune to such effects. However, it is important to understand that control theory optimization techniques and active feedback are extremely important here as in any linear collider e.g. in forming shaped bunches longitudinally and small bunches transversely in ways consistent with Liouville's theorem.

To maintain the overall phase coherence between cells, an electro-optical phase element can be included to control the phase and a group delay element to match individual cells to the electron(or positron) bunch in each cell. The spacing between linear arrays can contain active phase control elements such as one would need if they intended to use it for arbitrarily charged beam species. Although this suggests a very significant research development, the various technologies that are required are available now at reasonable costs and these are improving rapidly – at scales related to Moore's 'law'. This can not be said for the next generation RF structures either in terms of their fabrication technologies or their power sources because there is little, if any, commercial interest.

Acknowledgements

References

1. M. Stanley Livingston and John P. Blewett, *Particle Accelerators*, (McGraw-Hill, New York, 1962). Most recently see: Maury Tigner, Does Accelerator-Based Particle Physics Have a Future, *Phys. Today* **54** (Jan. 2001) 36.
2. J.E. Spencer, Real-Time Applications of Neural Nets, Proc. 6th Int'l. Conf. on Real-Time Comp. Appl's. in Nucl., Part. and Plasma Physics, Williamsburg, VA, May 16-19, 1989. *IEEE Trans. Nucl. Sci.* , Vol. **NS-36** (1989) 1485.
3. J.E. Spencer, Optimal Real-Time Control - Colliders, IEEE Part. Accel. Conf., Acc. Sci. & Tech. Vol. 91CH3038-7 (1991) 1440.
4. J.E. Spencer, Beam-Beam Effects and Generalized Luminosity, *Intl. J. Mod. Phys.* **11** (1996) 1675.
5. J.E. Spencer, Limitations Imposed by Beam-Beam Effects and Their Remedies, *Intl. J. Mod. Phys.* **13** (1998) 2479.
6. J.E. Spencer, Limitations Imposed by Beam-Beam Effects and Their Remedies - II, *Intl. J. Mod. Phys.* **15** (2000) 2543.
7. Power sources are presently available that could provide higher gradients than RF under this scenario at 50 MHz rep rates e.g. see the IMRA America, Inc. website.
8. Y.C. Huang et al, The Physics Experiment for a Laser-Driven Electron Accelerator, Nucl. Inst. Meth. A407 (1998) 316-321. T. Plettner et al, Status of the Laser Electron

Accelerator Project (LEAP), Quantum Aspects of Beam Physics, World Scient. Publ. Co., Singapore (1999) 310-321.

9. G. Dôme, Longitudinal and Transverse Wake-Fields of a Relativistic Particle in a Dielectric-Lined Structure, *Euro. Part. Accel. Conf.* (1990) 681.

10. Chris B. Schaffer, Andre Brodeur and Eric Mazur, Laser-Induced Breakdown and Damage in Bulk Transparent Materials Induced by Tightly Focused Femtosecond Laser Pulses, *Meas. Sci. Technol.* , **12** (2001) 1784.

11. The latest version of the cell is described in R.L. Byer et al., Progress of the Laser Electron Accelerator Project at Stanford University, IEEE Part. Accel. Conf., Acc. Sci. & Tech. (2001).

12. UV grade Fused Silica from CVI Laser Corp. was made by flame hydrolysis of silicon tetrachloride. Their catalog designation is RAP-50-UV.

13. Kyle B. Miller, James Leitch and Chandra Lyons-Mandel, Proton Radiation Testing of Optical Elements, *Nucl. & Space Rad. Effects Conf.* (2001) 155.

14. Zeroth-Order Design Report for the Next Linear Collider, May 1996, SLAC Report 474, LBNL-PUB-5424, UCRL-ID-124161.

15. J.P.H. Benschop, U. Dinger, D.C. Ockwell, EUCLIDES: First Phase Completed, SPIE Proc: Emerging Lithographic Technologies - IV, Vol. 3997 (2000) 34.

16. H.C. Pfeiffer, PREVAIL - IBM's E-beam Technology for Next Generation Lithography, ibidem, Vol. 3997 (2000) 206.

17. M.A. McCord, Introduction to Electron Beam Lithography, SPIE Int'l. Symposium on Microlithography (2000).

18. L. Ocala et al., PREVAIL - IBM's E-beam Technology for Next Generation Lithography, ibidem, Vol. 3997 (2000) 194.